Journal of *Marine Science and Engineering*

MDPI

Article

Development of AI-Based Multisensory System for Monitoring Quay Wall Events

Junsik Shin [1], Junyoung Park [1], Jongbin Won [1], Jongwoong Park [1,*] and Jiyoung Min [2,*]

[1] Department of Civil and Environmental Engineering, Chung-Ang University, Dongjak, Seoul 06974, Republic of Korea; jacoom1030@cau.ac.kr (J.S.); pjy5451@cau.ac.kr (J.P.); sac1721@cau.ac.kr (J.W.)
[2] Department of Structural Engineering Research, Korea Institute of Civil Engineering and Building Technology, Goyang-si 10233, Republic of Korea
* Correspondence: jongwoong@cau.ac.kr (J.P.); amote83@kict.re.kr (J.M.); Tel.: +82-2-820-5278 (J.P.)

Abstract: Structural monitoring of quay walls, where various events occur due to unexpected high waves, vessels, and heavy equipment, is essential. However, real-time events cannot be constantly monitored by on-site personnel. To resolve the aforementioned issues, this study proposes an innovative AI-powered, cloud-based wireless sensor system that incorporates a high-sensitivity accelerometer with an ultra-low noise level of 0.003 mg, designed to monitor the low response amplitude of massive quay walls. The sensor can be activated by a scheduled trigger or a long-rangefinder. Vessel detection is performed utilizing the AI-based object detection method, Faster R-CNN, which employs ResNet as the backbone network. The detected anchor box's position and dimensions are subsequently processed to confirm the presence of a berthing vessel. The collected data are then transmitted wirelessly to a proposed cloud server through LTE communication in real-time. The developed system was installed on a caisson-type quay wall in Korea, where acceleration, tilt, temperature, and camera image data were analyzed to assess its performance for real-time event monitoring. The results demonstrated that the safety of quay walls can be automatically managed by monitoring events during berthing and mooring with the proposed system.

Keywords: vibration-based monitoring; quay wall; AI object detection; multisensory system; berthing event

check for updates

Citation: Shin, J.; Park, J.; Won, J.; Park, J.; Min, J. Development of AI-Based Multisensory System for Monitoring Quay Wall Events. *J. Mar. Sci. Eng.* **2024**, *12*, 1902. https://doi.org/10.3390/jmse12111902

Academic Editors: Ziguang Jia, Peng Zhang and Yi Huang

Received: 21 August 2024
Revised: 22 October 2024
Accepted: 22 October 2024
Published: 24 October 2024

Copyright: © 2024 by the authors. Licensee MDPI, Basel, Switzerland. This article is an open access article distributed under the terms and conditions of the Creative Commons Attribution (CC BY) license (https://creativecommons.org/licenses/by/4.0/).

1. Introduction

In civil engineering, the development of advanced monitoring systems adapting cutting-edge technology for assessing structure conditions has significantly grown in response to the rising concerns about degradation and aging [1]. Port structures are no exception to this trend. These structures are particularly vulnerable compared to standard inland counterparts because of their unique environmental conditions. The presence of saline substances in coastal environments hastens the deterioration of materials, especially concrete and steel, commonly used in construction [2]. Additionally, unexpected high waves and irregular impact or friction forces induced by vessel berthing can further weaken these structures. Moreover, the effects of rampant climate change challenge the ability of port structures to endure throughout their lifespan [3].

For preemptive condition assessment of port structures, such as quay walls, visual inspection has traditionally been employed as a fundamental method. Visual inspections are performed periodically every three to six months to detect damage such as cracks and exfoliation. They are often inconsistent, labor-intensive, and influenced by the subjective judgment of the inspector. Direct access to underwater areas for inspection can be hazardous and is frequently hindered by turbid water and the presence of shells adhering to the surface. Choi et al. [4] and Ulrich et al. [5] proposed robot-based underwater inspection systems to replace human involvement. Hake et al. [6] introduced a scanning sensor system capable of assessing both above-water and underwater parts of the quay wall,

utilizing fully automated point cloud technology to classify damaged and undamaged zones. Additionally, Interferometric Synthetic Aperture Radar (InSAR) data have been used to measure deformation rates [7,8]. However, these visual inspection methods have a chronic limitation: they are inadequate for detecting damage immediately after it occurs, and the structural safety is assessed solely based on the severity of the damage observed afterward. In particular, for quay walls, various events such as high waves caused by typhoons, vessel berthing and mooring, and the use of heavy equipment on the upper structure occur frequently, making immediate monitoring and response necessary.

To enhance visual assessments, vibration-driven structural health monitoring (SHM) has been investigated to ensure structural safety and address unforeseen events. Many researchers have implemented Fiber Bragg Gratings (FBG) for quay wall monitoring [9–11]. Its high accuracy and precision are reliable, though it is difficult to install in the field and requires significant financial investment, which limits its applicability to general quay walls. With the rapid development of low-cost Micro-Electro-Mechanical Systems (MEMS), FBGs have the potential to be substituted. Zarafshan et al. [12] created a monitoring system for bridge scour by analyzing the vibration data in both time and frequency domains, collected from the bridge pier. While earlier approaches primarily focused on analyzing vibration data in the time and frequency domains, recent advancements have significantly enhanced the capabilities of vibration-based SHM. In particular, the integration of machine learning, deep learning, and advanced optimization techniques has led to more sophisticated methods for detecting structural damage, even in complex and dynamic environments. For example, Dang et al. [13] introduced a semi-supervised vibration-based SHM technique that uses deep graph learning to encode temporal relationships, dynamic features, and spatial correlations of sensor data, enabling high-accuracy damage detection even with limited labeled data. Similarly, Xiang et al. [14] applied machine learning with Bayesian optimization to enhance the precision of SHM for offshore wind turbines under varying environmental conditions. Fan et al. [15] proposed a one-dimensional convolution system based on vibration signals, showing how convolutional neural networks (CNNs) can process structural vibration data in real time for effective monitoring. Furthermore, Bel-Hadj et al. [16] and Kamariotis et al. [17] explored Bayesian approaches and operational modal analysis to estimate structural health based on vibration data, emphasizing the importance of continuous data collection and analysis to drive optimal maintenance decisions in SHM applications. These advancements demonstrate the growing integration of various technologies in the field of vibration-based SHM. However, for these advanced techniques to be effectively utilized, it is imperative to ensure the acquisition of accurate and high-quality vibration data. Without this fundamental prerequisite, the potential of these methods to detect and predict structural damage cannot be fully realized.

Despite progress in the SHM field, most related research has concentrated on inland structures like bridges and buildings, with limited attention to coastal structures due to various reasons: (1) The vibration level of a quay wall, due to its large mass, is too diminutive. Min et al. [18] explored a continuous vibration monitoring system using the ADXL354 MEMS accelerometer (Analog Devices, Inc., Cambridge, MA, USA) [19], which was implemented on a quay wall in Korea. However, they discovered that the collected data included minimal vibrational details, since the vibration level of the structure was significantly smaller compared to the sensor's resolution, rendering meaningful analysis unattainable. (2) Conventional sensing systems adopt continuous measurement to conduct vibration-based data-driven analysis. This is a common approach for the continuous monitoring of structures that can be excited by various load sources. However, for the extraction of excitation data in the case of quay walls, the main excitation source is the berthing impact of a vessel [20], which is very infrequent. Furthermore, it is difficult to distinguish the moment of berthing impact from single acceleration data. (3) This drawback also leads to an overflow of irrelevant data, which may waste server storage and often necessitates human involvement to parse and extract pertinent information. As a

result of these technological challenges, vibration-based SHM of quay walls has not been properly evaluated.

To address these issues, this study proposes an event monitoring system that includes berthing impact, which consists of three main subsystems: (1) a sensing system capable of measuring subtle vibrations adopting a high-sensitivity accelerometer; (2) AI and multi-sensor systems that accurately capture berthing impacts and long-term behavior; (3) a cloud-based system for automated data management and processing. The developed sensing system incorporates various sensors, featuring high-sensitivity acceleration, tilt, temperature, and distance measurement, and image acquisition for AI-based vessel detection. A specially designed triggering algorithm enables the system to accurately capture berthing impacts and long-term trends. This event-driven feature ensures efficient operation by focusing on key excitations necessary for vibration-based condition assessments. Additionally, the proposed cloud system is flexible and functions in real-time, enabling smooth integration with extra sensors and immediate on-site response in case of issues.

The remainder of the paper is structured as follows: Section 2 introduces the proposed berthing impact monitoring system. Section 3 describes the indoor experiments and field deployments, where the system's effectiveness was validated through extensive field tests in real-world port environments, confirming its practical applicability. Section 4 provides discussions, including preliminary analyses such as berthing pattern identification, natural frequency, and tilt extraction, which demonstrate the system's ability to provide foundational data for SHM of quay walls. These results suggest potential integration into existing or future SHM algorithms to enhance the safety of port structures. Finally, the conclusions are summarized in Section 5.

2. Development of a Quay Wall Monitoring System

To establish a sustainable health monitoring system for quay walls, a tailored wireless multi-sensor system was developed. The initial component of the proposed system is the trigger system, which is composed of two main mechanisms (Figure 1). The sensing system is activated based on the predefined logic of the trigger system. The sensing system operates intermittently, conserving power and avoiding the collection of irrelevant data. The sensing process begins with capturing an image using a connected webcam. A cloud-based AI object detection method, Faster R-CNN [21], trained on a custom dataset, is employed to swiftly identify the presence of a vessel within the image received through LTE communication. AI performs this additional verification despite the presence of a long-rangefinder (LRF) because it may not function properly under certain weather conditions when a vessel is berthing or unberthing. Based on the AI's prediction, the sensing duration is determined. If no vessel is detected, a shorter sensing duration is applied for long-term trend analysis. However, if a vessel is identified, the sensing time is extended to capture vibrations throughout the entire berthing, mooring, and unberthing process accurately. During the sensing process, various physical parameters are measured and the acquired data are wirelessly transmitted to the server, enabling automatic analysis. Upon completion of the process, the sensor switches to standby state, awaiting the next activation. The overall hardware configuration is shown in Figure 2. The functions of each hardware component, as well as their interconnections and operating principles, will be discussed in detail in Sections 2.1 and 2.2.

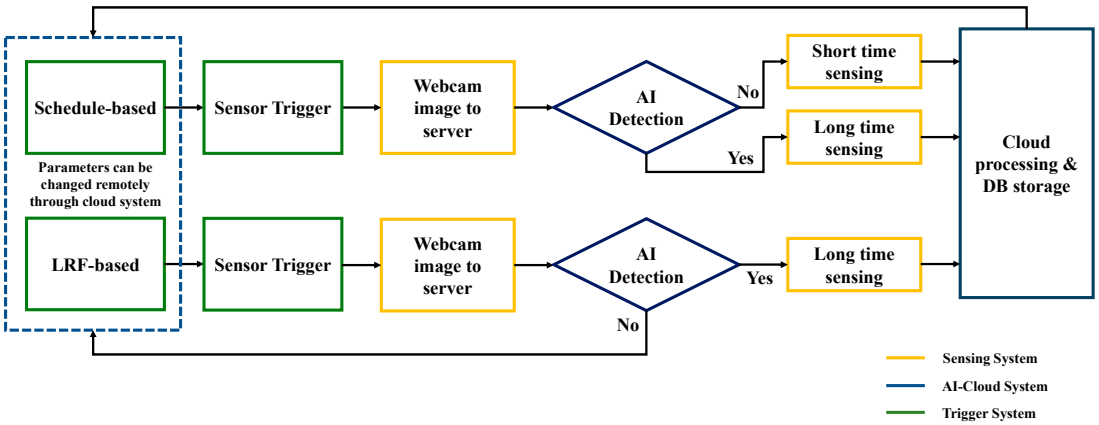


Figure 1. Flowchart of the proposed system.

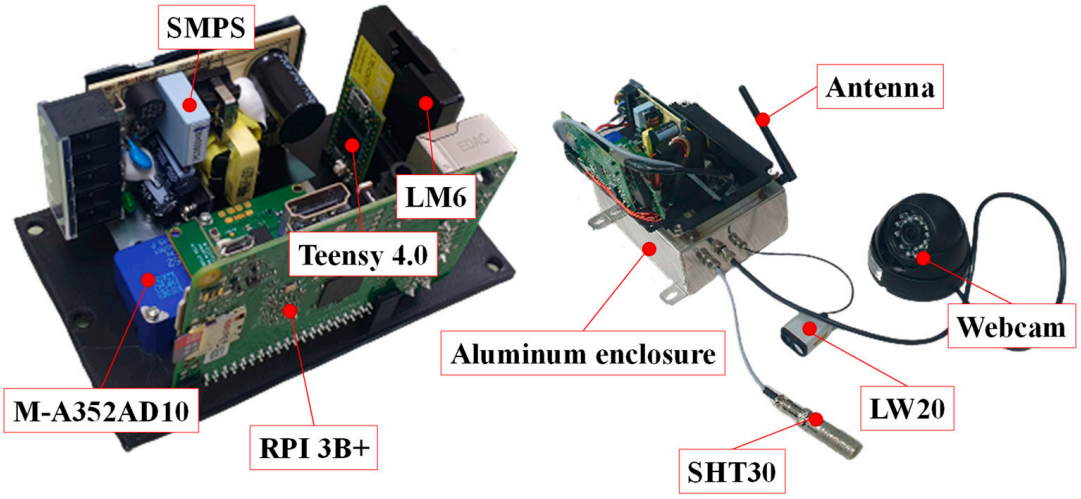


Figure 2. Overview of the hardware components in the proposed system.

2.1. Sensing System

2.1.1. MCU and Power Supply

The MCU functions as the central unit, overseeing the operation of connected sensors and managing the collected data. Therefore, selecting an appropriate MCU that meets the system's requirements is crucial. In the proposed design, the Raspberry Pi (RPI) 3B+ (Raspberry Pi Foundation, Cambridge, UK) [22] running a Linux operating system was chosen as the primary MCU from the options presented in Table 1. This MCU features a 1.4 GHz quad-core processor, well-suited for handling high-frequency data collection and processing tasks efficiently, without introducing delays. MCUs like Arduino Uno (Arduino, Torino, Italy) and ESP32 (Espressif Systems, Shanghai, China) were not suitable for multisensory data acquisition and real-time processing due to their resource limitations, such as lower memory and clock speed, which could lead to delays or system instability in high-frequency data environments. RPI 3B+ also offers multiple USB ports and various communication protocols such as Serial Peripheral Interface (SPI), Universal Asynchronous Receiver-Transmitter (UART), and Inter-Integrated Circuit (I2C), all of which are suitable for the proposed sensing system. Although the more recent model, RPI 4 (Raspberry Pi Foundation, UK) [23], was considered, its known overheating issues in outdoor applications could potentially lead to system failure, which made it less ideal for this use case.

Table 1. Specifications of general MCU models.

MCU Model	Processor	Clock Speed	RAM	Flash Memory	Power
RPI 3B+	Quadcore 1.4 GHz ARM Cortex-A53	1.4 GHz	1 GB (LPDDR2)	Up to 32 GB	5 V, 2.5 A
RPI 4	Quadcore 1.8 GHz ARM Cortex-A72	1.8 GHz	2 GB, 4 GB, 8 GB (LPDDR4)	Up to 32 GB	5 V, 3 A
Arduino Uno	8-bit AVR ATmega328P	16 MHz	2 KB (SRAM)	32 KB (Flash)	5 V
ESP32	32-bit Xtensa Dual-core LX6	240 MHz	520 KB (SRAM)	4 MB (Flash)	3.3 V
STM32F103C8T6 (STMicroelectronics, Plan-les-Ouates, Switzerland)	32-bit ARM Cortex-M3	72 MHz	20 KB (SRAM)	64 KB (Flash)	3.3 V
BeagleBone Black (BeagleBone.org, Oakland Twp, MI, USA)	ARM Cortex-A8	1 GHz	512 MB (DDR3L)	4 GB (eMMC, MicroSD)	5 V
Teensy 4.0 (PJRC, Sherwood, OR, USA)	32-bit ARM Cortex-M7	600 MHz	1 MB (SRAM)	2 MB (Flash)	5 V

The system's power supply was designed to operate in two different modes. When a reliable energy source is present in the field, a switched-mode power supply (SMPS) is utilized to activate the MCU. In locations where stable power is either unavailable or too costly, the second option is employed. In this case, integrated rechargeable lithium-ion batteries serve as a backup power source and are automatically engaged. These batteries are recharged through a solar panel connected to an LT3652 charging unit (Analog Devices, Inc., USA) [24]. Furthermore, the cloud computing and triggering methods implemented in the system help minimize power consumption, enabling efficient operation on relatively low energy.

2.1.2. High-Sensitivity Accelerometer

One of the primary challenges in vibration-based monitoring of quay walls is the low amplitude of the vibrations. Consequently, an accelerometer with high sensitivity and resolution was carefully chosen to address this issue. As shown in Table 2, five accelerometers were considered for the application. Among these, an accelerometer called EPSON M-A352AD10 (Seiko Epson Corporation, Suwa-shi, Japan) [25] was chosen, which provides digital tri-axial acceleration output along with exceptionally low noise, high stability, and low power consumption. Its ultra-low noise feature delivers a noise density of 0.2 $\mu G/\sqrt{Hz}$, a level of performance that is challenging to attain with standard MEMS accelerometers. In terms of sensitivity, its scale factor is 2^{-24} G/LSB, enabling the detection of even the most subtle vibrations. Other accelerometers were considered but showed limited noise density and sensitivity, which made them less suitable for detecting subtle vibration in quay wall environments. To initiate the sensing process, the MCU controls the accelerometer via a Python (version 3.9.2) script, with the sensing duration determined by the type of trigger (as described in Section 2.2).

Once the MCU triggers the sensing process, the accelerometer outputs tri-axial acceleration data at a 1000 Hz sampling rate. During data acquisition, a digital Finite Impulse Response (FIR) low-pass filter, specifically a Kaiser Filter with 128 taps and a 110 Hz cutoff frequency, is applied to eliminate high-frequency noise. The data are then downsampled to 100 Hz in real-time. During the sensing process, the data are simultaneously stored in a CSV file and transmitted to the server via the Message Queuing Telemetry Transport (MQTT) protocol (as detailed in Section 2.3.1). In Figure 3, the process of acquiring high-sensitivity acceleration data is illustrated in the form of a flowchart. The dashed arrow in the figure indicates the hardware connection between the MCU and the accelerometer.

Table 2. Specifications of general accelerometer models.

Accelerometer Model	Type	Range (g)	Noise Density	Sensitivity	Output Data Rate
M-A352AD10	MEMS (3-axis), Digital	±15	0.2 μg/√Hz	0.06 μg/LSB	1 kHz
ADXL354	MEMS (3-axis), Analog	±8	22.5 μg/√Hz	400 mV/g	1 kHz
LIS3DHH (STMicroelectronics, Switzerland)	MEMS (3-axis), Digital	±2.5	45 μg/√Hz	76 μg/LSB	1.1 kHz
SCA3300 (Murata Manufacturing Co., Ltd., Kyoto, Japan)	MEMS (3-axis), Digital	±6	37 μg/√Hz	370 μg/LSB	2 kHz
BMA400 (Bosch Sensortec, Reutlingen, Germany)	MEMS (3-axis), Digital	±16	300 μg/√Hz	980 μg/LSB	800 Hz

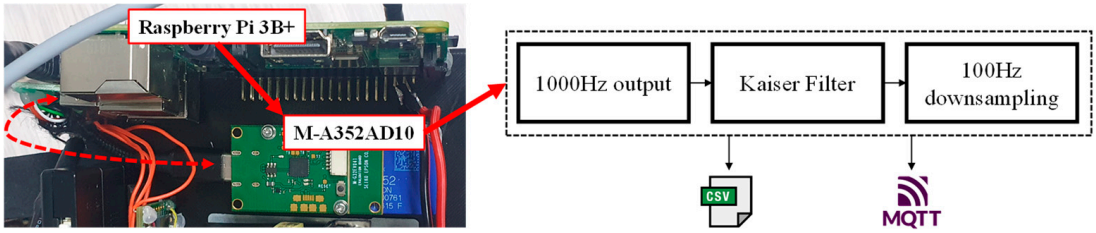


Figure 3. Proposed acceleration acquisition process.

2.1.3. Tilt Estimation from Acceleration

The inclination of a structure offers important insights into its long-term stability. While a dedicated inclinometer could be used to measure tilt, it is possible to estimate the tilt based on the recorded acceleration data. As a result, it is beneficial to compute the tilt simultaneously during acceleration measurements. The method for estimating tilt from acceleration is represented in Equation (1):

$$\theta = \arctan\left(\frac{a_x}{\sqrt{{a_y}^2 + {a_z}^2}}\right), \psi = \arctan\left(\frac{a_y}{\sqrt{{a_x}^2 + {a_z}^2}}\right) \quad (1)$$

where θ and ψ represent pitch and roll angle, respectively; a_x,a_y, and a_z represent the acceleration along the x, y, and z axes, respectively. While the accelerometer effectively estimates the pseudo-static tilt component, its accuracy in capturing the dynamic tilt component is constrained by translational accelerations, such as those caused by structural vibrations, as well as signal interference from sensor crosstalk. To address this issue, Liu et al. introduced a complementary filter that merges accelerometer data, which detects the pseudo-static tilt component, with gyroscope data for improved dynamic component measurements. Liu's experiments also demonstrated that tilt within the frequency range of 0.001–0.1 Hz can be effectively measured using an accelerometer [26]. Consequently, the developed sensing system incorporates a real-time low-pass filter featuring a 1 Hz cutoff frequency to guarantee accurate acquisition of tilt data.

2.1.4. Thermometer and Webcam

Additionally, an SHT30 thermometer (Sensirion, Stäfa, Switzerland) [27] was integrated into the sensing system due to its ability to meet the target specification of 0.2 °C accuracy and its operational temperature range of −40 to 125 °C. Temperature is a key factor in understanding the relationship between structural behavior and thermal fluctuations. Since the thermometer lacks waterproofing, a custom-made 3D-printed casing was designed to protect it from water exposure in the field. SHT30 was interfaced with the main MCU via the I2C, with data gathered once per triggering event. Capturing images at the site represents another essential element for vessel detection. To facilitate efficient

image capture of the site, a webcam was integrated into the system alongside the RPI 3B+. This waterproof webcam (Ailipu Technology Co., Ltd., Shenzhen, China) offers a 5 MP resolution and includes infrared functionality for capturing images in low-light or nighttime conditions.

2.2. Trigger System

The proposed trigger system is designed to activate the sensing mode. This mechanism allows for the accurate detection of vibrations specifically associated with berthing or other events, while also enabling the collection of data for long-term trend analysis. It minimizes unnecessary data accumulation and reduces power usage. The trigger system comprises two main components: a predefined schedule and a system based on a long-rangefinder. Both components work together in a complementary way to ensure efficient and precise data collection.

2.2.1. Predefined Schedule-Based

The primary objective of the predefined schedule-based trigger is to collect periodic long-term trend data and observe the sensor's condition. This trigger is managed by an internal threading timer module within a Python script. When the timer is activated, the sensor immediately switches to sensing mode, and the images captured are transmitted directly to the cloud server for AI-based object detection. Depending on the server's detection results, the system adjusts the sensing period, such as 30 s if no vessel is identified and 20 min when a vessel is detected. Additionally, parameters like the trigger interval and sensing period can be configured remotely by updating the MySQL (version 8.0.20) database on the server. This schedule-based approach not only aids in long-term data collection but also compensates for the limitations of the long-rangefinder-based trigger method mentioned in Section 2.2.2. Although the long-rangefinder method accurately identifies mooring times using distance measurements, it may encounter issues under adverse external conditions like severe weather. The predefined schedule-based approach mitigates these challenges, ensuring reliable and continuous data collection.

2.2.2. Long-Rangefinder-Based

To enhance the accuracy of detecting the timing of vessel berthing, a long-range distance sensor was utilized. The LW20 model (LightWare LiDAR Inc., Boulder, CO, USA) [28], featuring IP67 waterproofing and capable of measuring distances up to 100 m with a resolution of 1 cm, was selected. Unlike conventional rangefinders, the LW20 product offers robust dust penetration through its first and last pulse detection technology, enabling it to maintain optimal performance even under challenging environmental conditions such as dust, mist, fog, rain, snow, and bright sunlight. An external MCU, the Teensy 4.0 (PJRC, USA) [29], was utilized to manage the acquisition of distance data from the rangefinder. This standalone system was developed to activate sensing based on distance, thereby reducing the processing load on the primary MCU, the RPI 3B+. Additionally, the lower power consumption of the Teensy 4.0 compared to the RPI 3B+ made it suitable for the continuous operation of the rangefinder. The LW20 rangefinder was interfaced with the Teensy 4.0 using the I2C protocol, and the collected data were sequentially transferred to the RPI 3B+ at a rate of 1 Hz. The system uses a preset distance threshold to activate sensing based on vessel berthing and unberthing activities. This parameter can be updated wirelessly via MySQL, similar to the system described in Section 2.2.1.

2.3. AI-Cloud System

2.3.1. Wireless Communication System

Quay walls present accessibility challenges due to strict security and safety restrictions. Consequently, implementing a reliable wireless communication system to prevent data loss is crucial. Leveraging the latest developments in wireless communication technology, the LM6 modem (M2MNET, Anyang, Republic of Korea) [30] was chosen, offering advanced

LTE CAT 1 capabilities. This modem enables upload and download speeds of up to 10 Mbps, allowing for real-time transmission of data and images to the server. It is linked to the RPI 3B+ via a USB connection. To reduce the potential for data loss, data are sent using two distinct methods. The first method transmits time-series data in real time using the MQTT protocol by employing AT commands provided by the modem. The data are bundled into batches of 5 rows in JSON format and transmitted to the server under a specified topic. The second method involves sending a CSV file containing all data and associated JPG images directly to the server. In this scenario, the USB networking mode is used to connect the RPI 3B+ to the internet.

2.3.2. Cloud Processing and Database

An Amazon Elastic Compute Cloud (EC2) instance operating within an Ubuntu (22.04.4 LTS) environment was set up. The server's architecture incorporates several components, including Flask (version 2.0.1), Node.js (version 18), InfluxDB (version 1.6.7), PyTorch (version 1.10.1), and MySQL. Flask is used to receive JPG and CSV files from the sensor. When the sensor sends a request to its remote URL, the server organizes and stores the JPG and CSV files in a predetermined directory, sorted by vessel presence and sensor ID. Additionally, Flask plays a crucial role upon receiving image data: it initiates a PyTorch-based Faster R-CNN inference model utilizing pre-trained weights for vessel detection (as detailed in Section 2.3.3).

Node.js manages the real-time transmission of data through MQTT. The server's MQTT broker, powered by Mosquitto (version 2.0.11), is configured to listen to all topics provided by the sensor using the MQTT wildcard feature. Sensor data from various nodes are aggregated and processed based on subtopics, involving organizing the data into columns and transferring them to InfluxDB, a time-series optimized database.

Data from each sensor are categorized into primary and secondary sections. Primary physical quantities (triaxial acceleration, tilt) are logged under the schema named "sensor#" (where "#" indicates the sensor ID) in InfluxDB. Secondary data, including trigger time, distance, temperature, and trigger type, are recorded in the "sensor#_info" schema. MySQL is primarily used to handle remote sensor management in the field. The sensor system is configured to periodically access the MySQL database by performing queries under specific conditions, enabling automatic parameter adjustments and evaluation of object detection results without manual control.

Furthermore, this database structure is designed with scalability in mind, ensuring that the system can seamlessly accommodate an increased number of sensors without requiring significant modifications. Figure 4 provides a detailed description of the cloud computing algorithm flow.

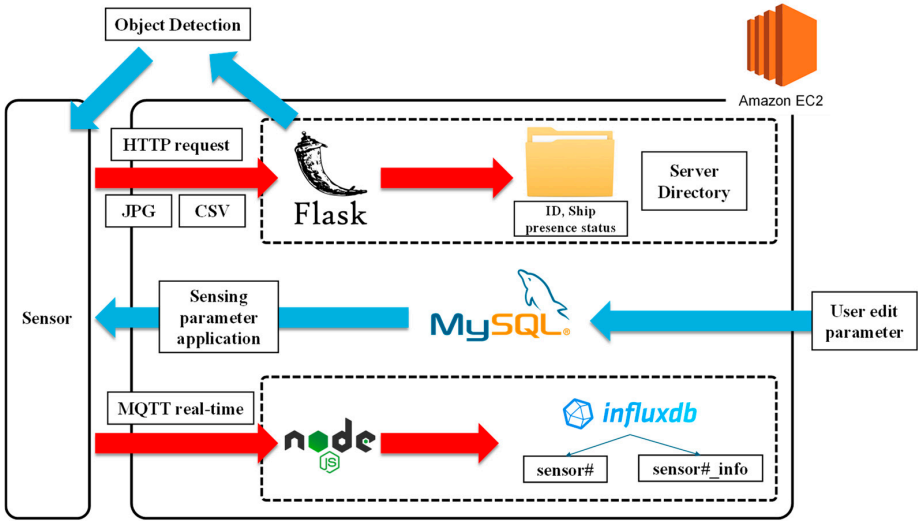


Figure 4. Proposed AI-Cloud system flowchart.

2.3.3. Vessel Detection Using Faster R-CNN

Once the trigger system is activated, the sensor must detect the presence of a vessel to adjust the sensing duration accordingly and allocate the database correctly. To achieve this, AI techniques, particularly object detection, have been employed. The object detection method used is known as Faster R-CNN, designed by a development team at Microsoft. Faster R-CNN builds upon R-CNN and Fast R-CNN, significantly enhancing the accuracy and speed of object detection and classification. The key advancement of Faster R-CNN is the introduction of the Region Proposal Network (RPN) and anchor boxes, which substantially reduce computational time and enable end-to-end training of the network.

For training the model, an initial dataset was created through web image crawling on Google. A total of 233 images containing vessels were gathered and labeled before being input into the network. The labeling was conducted using a Python annotation tool (napari 0.4.16), and the ground truth bounding boxes were marked with the label "Ship". Of the dataset, 80% was allocated for training with the remaining 20% equally split between validation and testing datasets. Figure 5 depicts the structure of the Faster R-CNN network and illustrates how it processes images for training and object detection.

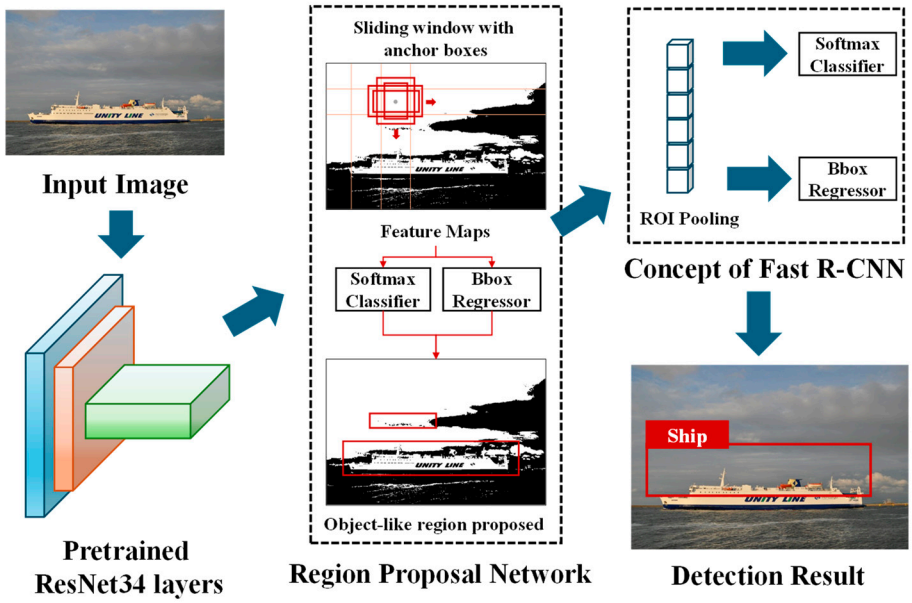


Figure 5. The structure of the Faster R-CNN model introduced in this study.

The pre-trained ResNet-34 [31] was employed for feature extraction. Preprocessing was performed to adjust the input images to 1024 × 1024 pixels, and the mean and standard deviation values typically employed in ImageNet training were used for image normalization. Additionally, data augmentation methods, including horizontal and vertical flipping, were utilized during the conversion process. As for the anchor boxes, five distinct sizes and three aspect ratios were selected. The selection of anchor boxes with various sizes and aspect ratios contributed to improved detection of diverse vessel sizes and orientations. The Intersection over Union (IoU) threshold, defined in Equation (2), was employed for evaluation.

$$IoU(B_1, B_2) = \frac{B_1 \cap B_2}{B_1 \cup B_2} \quad (2)$$

where B_1, B_2 represent the ground truth and predicted bounding box areas, respectively. A threshold of 0.5 was implemented to distinguish true positives from false positives. Comprehensive details of the parameters employed during training are presented in Table 3.

Table 3. Parameters used for training the model.

Parameter	Value
Conv network	ResNet-34
Input Image Size	1024 pixel
Image mean	[0.485, 0.456, 0.406]
Image std	[0.229, 0.224, 0.225]
Batch size	2
Learning rate	0.001
Maximum epochs	500
Anchor size	[32, 64, 128, 256, 512]
Anchor aspect ratio	[0.5, 1.0, 2.0]
IoU threshold	0.5
Patience	50

An early stopping technique was used during the training process to optimize model training and prevent overfitting. Validation was performed at each epoch, and the average precision (AP) was computed. If the AP for the validation set declined, the model was flagged as overfitting. At that point, a checkpoint was saved, and the model was allowed an additional 50 epochs (patience) to assess potential improvement. If no improvement was observed within this period, training was terminated early, and the model with the best performance (based on the checkpoints) was chosen.

A checkpoint was saved at epoch 44, step 4184. Over the subsequent 50 epochs of patience, no enhancement in the model's performance was observed. As a result, training stopped early at epoch 94, instead of proceeding to the full 500 epochs. The model saved at epoch 44 was selected as the best. Testing on 24 images from the test set produced an AP of 0.92, indicating a high degree of accuracy. Figure 6 provides logs of the loss variations throughout the training process.

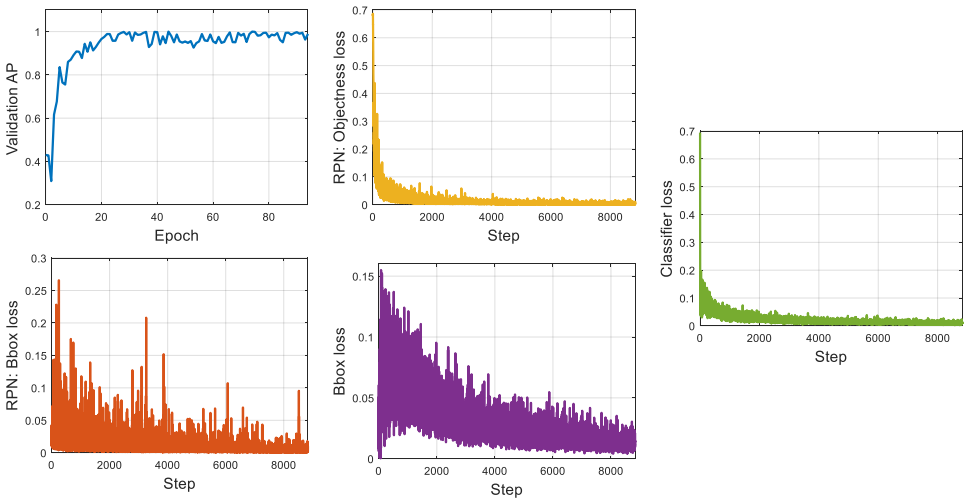


Figure 6. Variation of Loss and AP curves during the model's training.

Figure 7 presents the inference results produced by the trained model. The images presented were excluded from the model's training phase. The outcomes demonstrate that the trained model effectively detects vessels and pinpoints their positions within the image using bounding boxes. The model was implemented on a cloud server and the processing duration for inferring a single image on the server was around 0.2 s, demonstrating the feasibility of real-time vessel recognition. Leveraging transfer learning, the model successfully detected vessels with high accuracy, even when trained on a relatively small dataset.

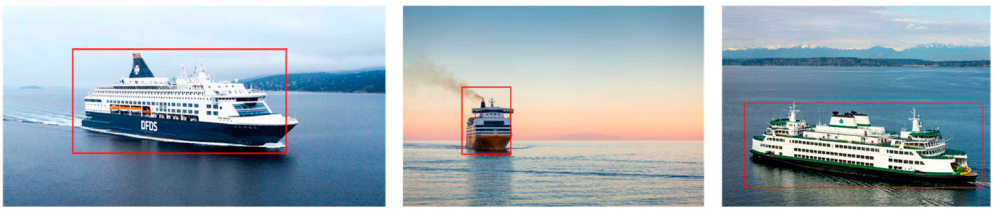


Figure 7. Inference result of random vessel image (Red boxes represent detected region).

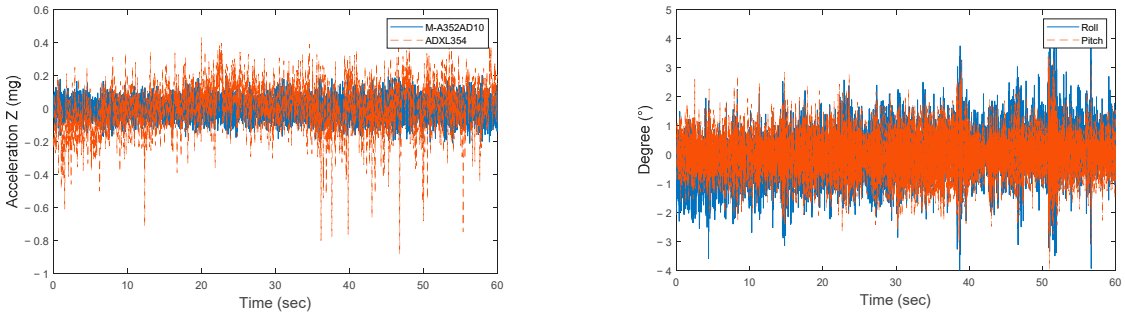
Faster R-CNN was chosen for the main object detection algorithm as it satisfies the balance between target accuracy and inference speed. Utilizing object detection provides a significant advantage in acquiring image data, which can be leveraged for various analyses and ultimately enhances the overall monitoring capabilities of the system. However, like all object detection algorithms, Faster R-CNN is susceptible to environmental effects such as poor visibility, reflections, and weather conditions. To address these challenges, the proposed cloud-based system allows for continuous learning and improvement of the model using the collected data. Moreover, it facilitates easy upgrades to state-of-the-art models as they become available. Through this approach, it is expected that the system will progressively overcome environmental influences and improve its detection accuracy.

Furthermore, the system's reliability is enhanced by the integration of a rangefinder, which works alongside the object detection model to provide additional verification and cross-validation. Additionally, as multiple images are captured throughout the berthing process, the combination of rangefinder data and repeated image capture significantly improves the accuracy of vessel detection and ensures reliable performance.

3. Experimental Validations

3.1. Indoor Experiment

An experimental evaluation of the proposed accelerometer's performance was conducted by comparing its noise floor to that of a standard MEMS accelerometer, the ADXL354. Both accelerometers were situated in a vibration-free environment, and data were recorded concurrently for a duration of one minute at a sampling frequency of 100 Hz. The root mean square error (RMSE) for the noise detected by the ADXL354 was 0.1 mg, while that for the M-A352AD10 was 0.003 mg. This experiment validated that the proposed sensing system can detect extremely low vibration levels, with sensitivity roughly 30 times higher than that of a conventional MEMS accelerometer as shown in Figure 8a.



(**a**) (**b**)

Figure 8. (**a**) Noise level of ADXL354 and M-A352AD10; (**b**) roll and pitch noise level of the M-A352AD10.

Experiments were carried out to evaluate the real-time performance of tilt measurements derived from acceleration, utilizing the PRMTZ8/M high-precision rotation stage (Thorlabs, Inc., Newton, NJ, USA) [32] at Hanbat University, Republic of Korea (Figure 9). The tilt readings from the rotation stage were then compared with those recorded by the sensor. For accuracy validation, two test scenarios were performed: one with tilts ranging

from 0 to 25 degrees in 5-degree increments and another involving micro-level tilts. As shown in Table 4, the developed sensor demonstrated an error margin of 1.4% and 1.67% across the two scenarios, validating its ability to accurately measure tilt. Additionally, the noise levels for roll and pitch tilts were measured under vibration-free conditions, similar to the acceleration tests. Figure 8b displays the measured noise, with RMSE values of 0.0009° for roll and 0.0008° for pitch, indicating the sensor's high sensitivity for tilt measurements.

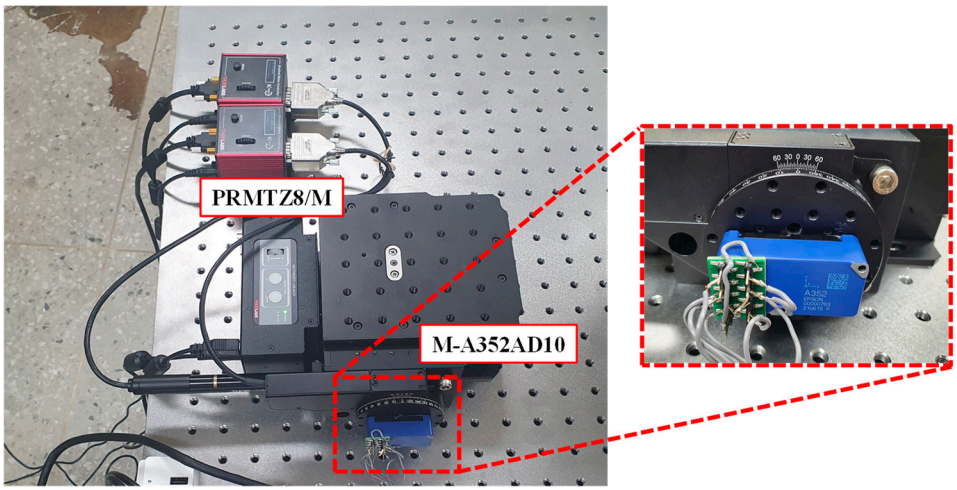


Figure 9. Experimental configuration for tilt validation.

Table 4. Comparison of tilt measurements between the rotation stage and the developed sensor.

PRMTZ8/M (°)	M-A352AD10 (°)	Difference (°)
1.000	0.989	0.011
0.100	0.101	0.011
0.010	0.010	0
0.001	0.001	0
5.000	4.916	0.084
10.000	9.924	0.076
15.000	14.934	0.066
20.000	19.930	0.070
25.000	24.826	0.174

3.2. Field Application and Challenges

The quay wall environment presented unique challenges for sensor deployment, requiring careful consideration. During the initial field investigation, it was observed that the impact of dust and salt was more significant than anticipated, while the initial design of the sensor casing focused primarily on waterproofing. Consequently, the system underwent extensive revision, with all components upgraded to meet an IP67 rating. This included redesigning sensor casings, cable glands, and protective corrugated tubes to achieve resistance to both water and dust infiltration. Other challenges were encountered with cameras and rangefinders, which are susceptible to environmental contamination compared to others. Over time, the accumulation of dust and salt on the lens caused a gradual degradation in image and measurement quality. To address this issue, protective coating was applied to the lenses, enhancing their resistance to contamination and ensuring sustained performance. Also, to eliminate intermittent signal interference detected from the rangefinder, the trigger algorithm was refined to activate when a signal exceeding the threshold persists for more than 10 occurrences, significantly reducing the occurrence of false triggers.

During the initial field investigation, the resistance of the proposed system to environmental effects was validated. As shown in Figure 10, the acquired image data were

severely corrupted due to the impact of snow and rain, which limited the performance of the AI-based vessel detection system. Since object detection techniques heavily rely on image quality, such challenges may arise regardless of how advanced the model is. Despite these difficulties, the proposed system accurately detected the berthing and unberthing of vessels, thanks to its multisensory integration. As illustrated in the graph, changes in distance measurements were observed, allowing for precise berth prediction even in extreme environmental conditions. Additionally, frequency domain analysis of vibration data, as outlined in Section 4.2, provides a method for distinguishing vessel types, even when visibility is limited. These results confirm that the proposed system compensates well for the strengths and weaknesses of various elements of the system, ensuring robust operation even under adverse environmental conditions.

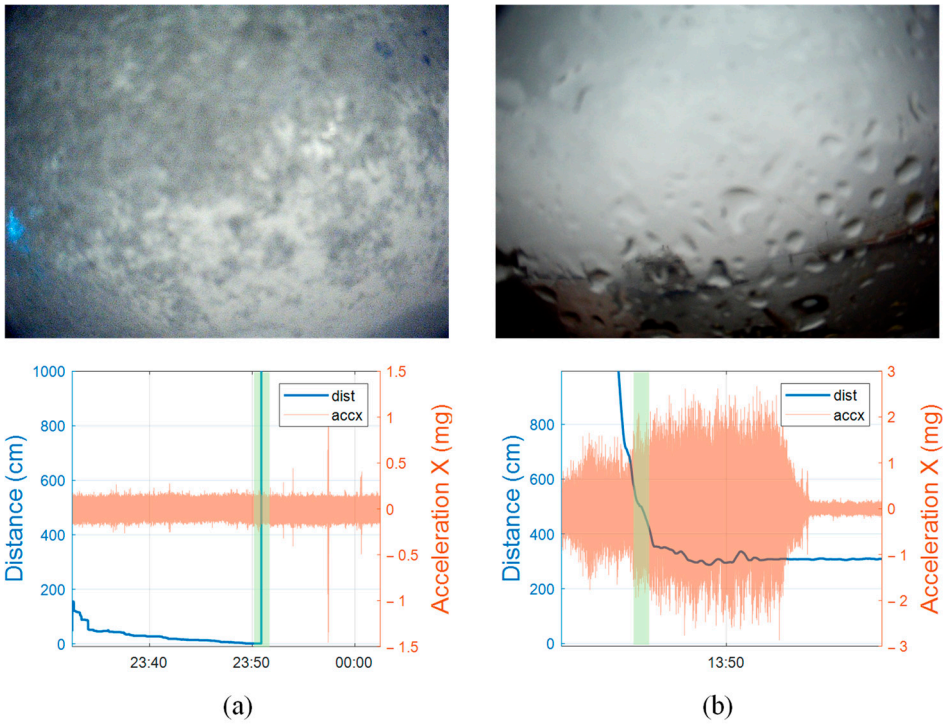


Figure 10. AI object detection limited by environmental factors: (**a**) snow (unberthing case); (**b**) rain (berthing case). Green line indicates berthing/unberthing timing.

These real-world challenges and the subsequent system adaptations highlight the importance of designing a robust monitoring system that can withstand the complex environmental conditions of the quay wall. The proposed sensing system demonstrated reliable performance through these iterative improvements, offering valuable insights for future enhancements in quay wall monitoring technologies.

The proposed sensing system was deployed at a caisson-type quay wall in Korea. Positioned adjacent to the fender system that reduces berthing impact, the sensor was anchored to the ground using bolts. Constant power was provided, and both the webcam and LRF were aligned according to the expected berthing direction. This deployment acted as an initial exploration to evaluate the feasibility of the proposed system under actual conditions.

The system was set up on 21 July 2023 and later dismantled on 6 August 2023. Figure 11 illustrates the installation configuration. For the LRF trigger, a 5 m threshold was set to recognize berthing and unberthing events. For the predefined schedule-based trigger, a trigger interval of 30 min was applied. When a vessel was detected by the proposed algorithm, the sensing time was set to 20 min; otherwise, it was set to 30 s. Figure 12 shows the orientation of acceleration and tilt measurements.

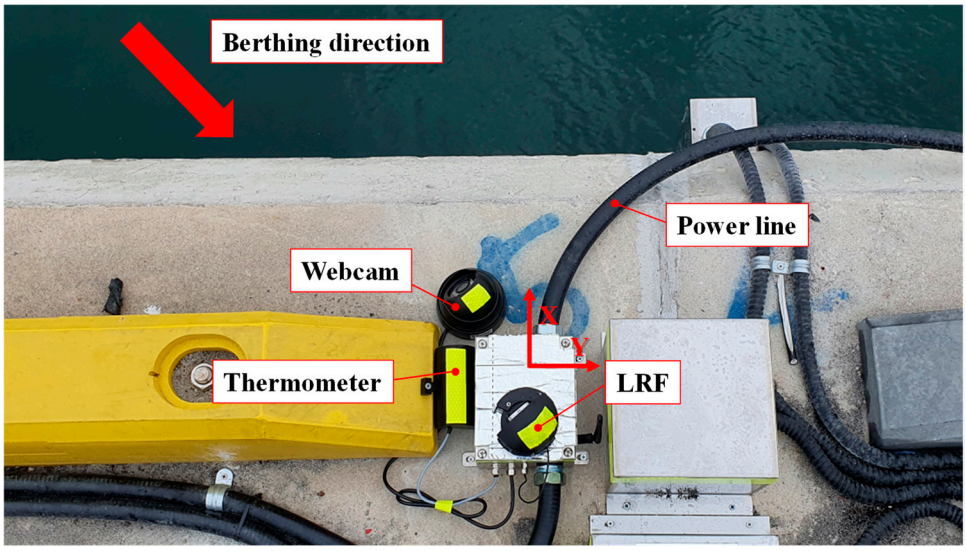


Figure 11. Deployment of the proposed sensing system in the field.

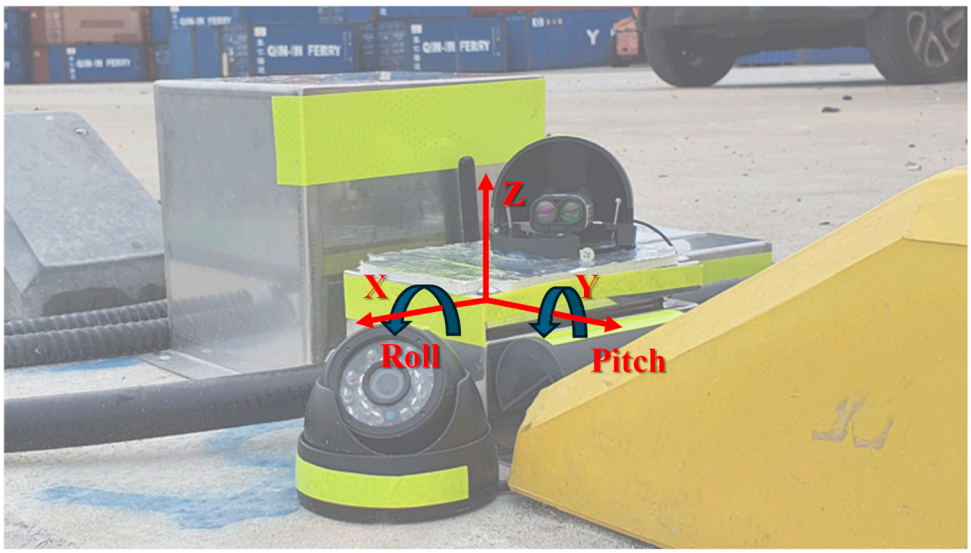


Figure 12. Definition of acceleration and tilt orientation.

4. Discussion

4.1. Vessel Detection Results

A key challenge faced during the field application of the vessel detection algorithm was the presence of multiple vessels within a single frame. This raised the risk of the algorithm incorrectly identifying a stationary or transiting vessel as a berthing event, as demonstrated by the image captured on 22 July (Figure 12). To address this issue, the detection algorithm was adjusted to limit the detection area within the image to specific regions of interest. This improved accuracy by focusing on areas where vessel berthing is most probable.

During the measurement period, a total of 12 berthing/unberthing events were detected and recorded based on the data collected on the cloud server. As shown in Figure 13, images corresponding to these times confirmed that the vessels were indeed berthing. Additionally, by cross-referencing the shared schedule, it was verified that there were exactly 12 berthing/unberthing events during the measurement period, confirming that the proposed algorithm successfully captured the berthing/unberthing data. Furthermore, it was confirmed that the data from the start of berthing to unberthing were successfully recorded (the green section in Figure 14 indicates the time when the photo was taken).

The ability to compare distance data and vibrations simultaneously during the mooring process suggests that this information could be valuable in future analyses, particularly in evaluating the effects related to distance. Moreover, the appearance on the image footage revealed only two types of vessels moored at the target quay wall. In this paper, these two types of vessels will be referred to as Type A and Type B.



Figure 13. Images of detected vessels through the proposed system. (Red boxes represent detected region).

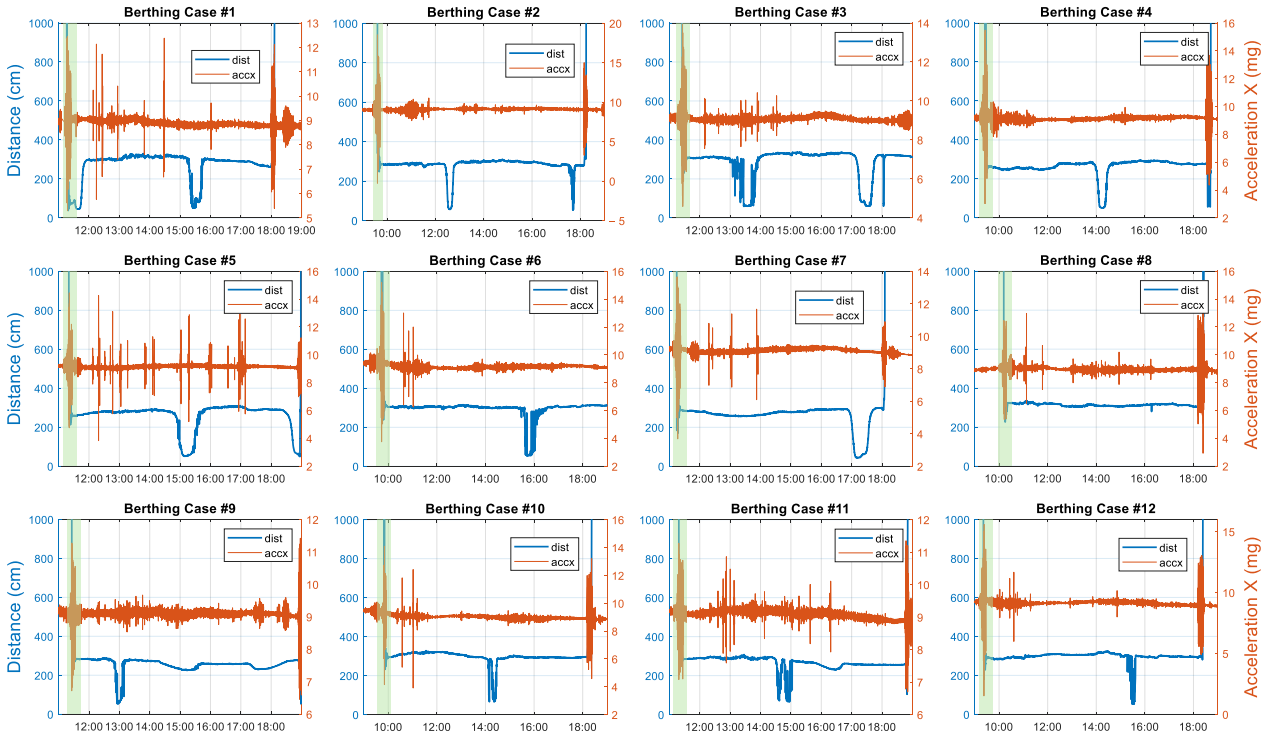


Figure 14. Acceleration and distance data measured during the berthing/mooring/unberthing process.

4.2. Berthing Vibration Analysis

Basic analysis was conducted on one of the 12 berthing events to assess whether the measured data could be utilized in various existing and state-of-the-art SHM techniques.

It was observed that most of the vibrations during berthing originated from the vessel's thruster, and the gradual decrease in amplitude over time confirmed that the thruster had been turned off. Subsequently, a significant impact vibration was observed, which was identified as the result of a collision between the vessel and the quay wall's fender, being towed by a tugboat (Figure 15). These impact data, along with the thruster vibrations, are expected to be crucial for vibration-based structural health monitoring, which can be further utilized to analyze trends in structural frequency and stiffness changes.

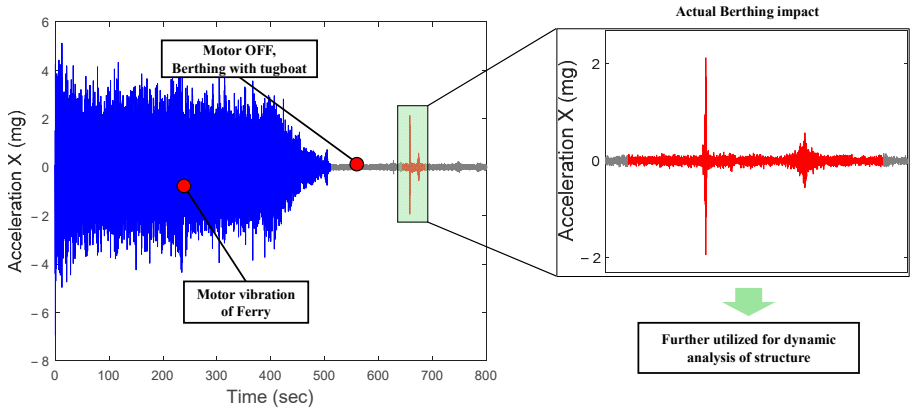


Figure 15. The composition of berthing vibration measured on the quay wall.

Upon examining the amplitude of each axis in the berthing data, it was found that the largest amplitude occurred in the x-axis direction, which corresponds to the vessel's approach. The maximum amplitude in the x-axis observed during the mooring process ranged between approximately 2 mg and 10 mg (Figure 16). Additionally, a cross power spectral density (CPSD) analysis of the mooring vibration data for two categories of vessels, Type A and Type B, revealed that vessels of the same type exhibited similar frequency spectra (Figure 17). This suggests that each vessel has a unique motor frequency, which enables the differentiation of vessel types through vibration data analysis in the frequency domain, even in situations where visibility is limited. Additionally, the dominant frequency commonly found around 15 Hz is likely related to the natural frequency of the structure. Based on these results, it has been verified that frequency analysis of the quay wall using the proposed system is feasible and tracking the maximum vibration level can further assist in setting thresholds for monitoring and detecting anomalies in the structure.

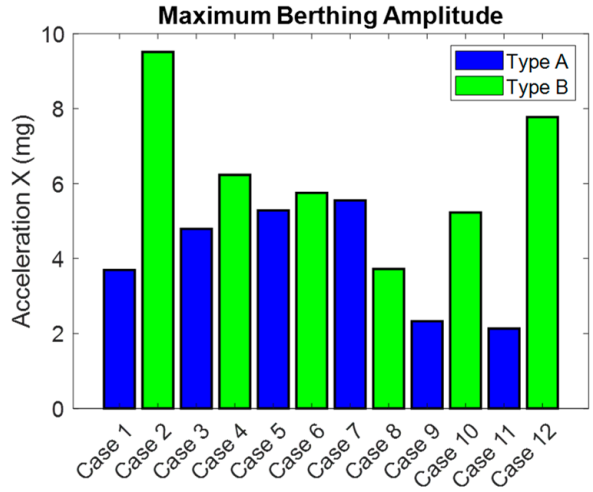
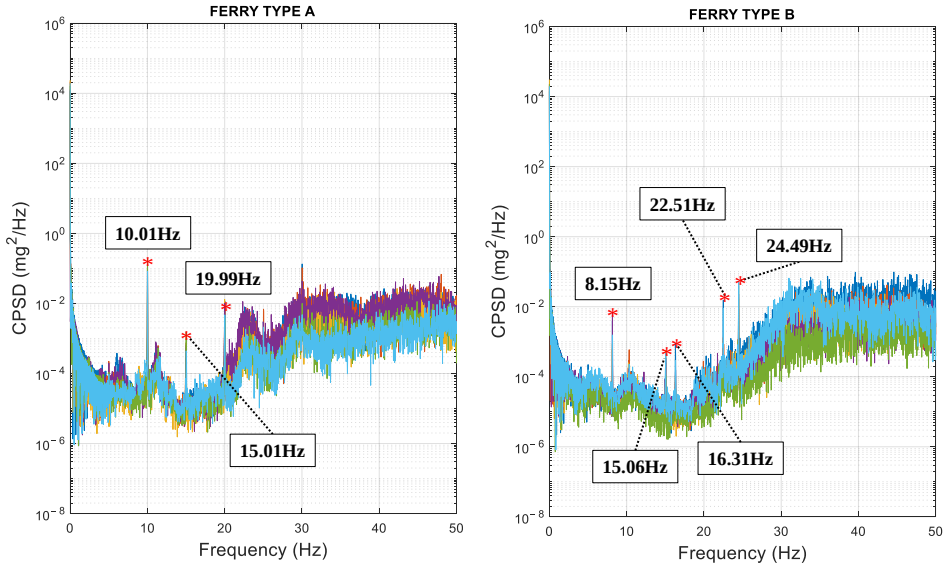


Figure 16. Maximum x-axis acceleration observed (Type A and Type B).



(**a**) (**b**)

Figure 17. Cross power spectral density of (**a**) berthing vibration of vessel Type A and (**b**) berthing vibration of vessel Type B. (Different colors represent individual cases).

4.3. Long-Term Tilt and Temperature Analysis

Throughout the application period, the predefined schedule-based trigger functioned effectively, with the data collected on the Flask server consistently showing 30 min intervals when no vessel was detected. The long-term data were analyzed based on these schedule-based triggers, which collected data at regular intervals, enabling an investigation into the correlation between temperature and tilt. During the measurement period, pitch exhibited a slight variation of approximately 0.0565 degrees while roll showed a change of 0.02 degrees, as shown in Figure 18. When these variations were plotted against temperature, some nonlinear correlations were identified. A cubic regression analysis revealed a coefficient of determination of 0.763 for pitch and 0.524 for roll, indicating that pitch is more closely related to temperature. If such data are collected over an extended period, it could serve as a critical indicator of structural damage, particularly if the tilt deviates from expected ranges at specific temperatures.

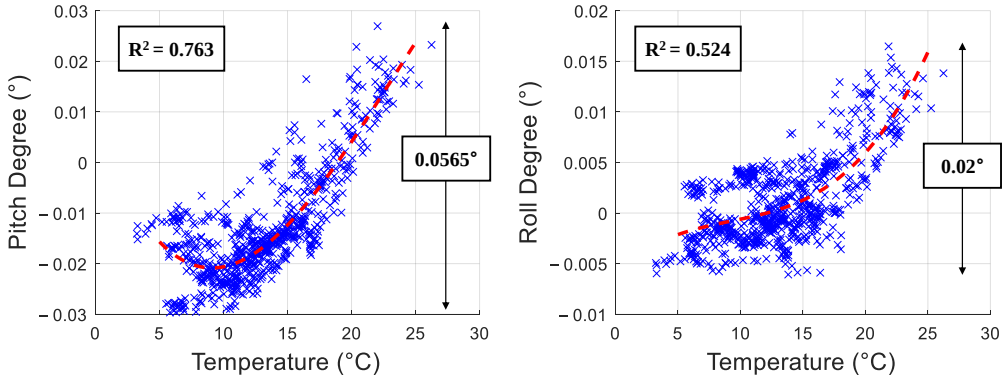


Figure 18. Relationship between tilt and temperature changes.

5. Conclusions

This paper discusses the development of an optimized AI-cloud-powered wireless sensing system tailored for monitoring the structural health of port infrastructure, with a particular emphasis on quay walls. Unlike inland structures, quay walls face unique challenges due to their exposure to coastal environments, which accelerates structural

degradation. Traditional vibration-based structural monitoring has been limited regarding port applications due to the massive mass of quay walls, leading to diminutive vibrations that are difficult to detect with conventional sensors. Additionally, commonly used constant sensing systems result in significant energy consumption and the collection of excessive, irrelevant data, complicating data processing and requiring frequent human intervention.

In response to these challenges, this study presents an innovative monitoring system that integrates cutting-edge technology, including the EPSON M-A352AD10 accelerometer, which features an ultra-low noise density of 0.2 $\mu G/\sqrt{Hz}$ and a high sensitivity scale factor of 2^{-24} G/LSB. The system also includes a tilt estimation technique based on acceleration measurements, providing valuable information on structural stability without the need for additional sensors. Laboratory tests demonstrated the high sensitivity and accuracy of the proposed system for detecting the minimal vibrations typical of quay walls.

A key innovation of this system is its event-triggered data acquisition approach, which minimizes unnecessary data collection and power consumption by activating the sensors only during significant events, such as vessel berthing. The system employs a dual-trigger mechanism: a predefined schedule-based trigger for long-term trend analysis and a long-rangefinder-based trigger for real-time detection of berthing events. To ensure accurate detection of vessel presence, the system integrates AI-based object detection using a custom-trained Faster R-CNN model, which achieved an average precision (AP) of 0.92 on the test dataset.

For wireless communication, the system utilizes state-of-the-art LTE CAT 1 technology, enabling reliable and efficient transmission of data to the server with sufficient bandwidth for real-time monitoring. This ensures robust communication even in challenging port environments. All data processing, including vessel detection, vibration analysis, and system management, is fully automated and handled through the proposed cloud system. The cloud system not only processes the data but also stores them systematically and provides real-time feedback, enabling remote control and analysis without the need for on-site human intervention.

The system was successfully deployed at a quay wall in Korea, where it effectively monitored 12 berthing events over the installation period. The collected vibration data, along with tilt and temperature measurements, were automatically processed and analyzed through the cloud system, demonstrating the feasibility of vibration-based condition assessment for port structures. Analysis of the data revealed consistent vibration patterns during berthing, indicating the potential of using this system to monitor structural health and detect anomalies over time.

Future research should focus on extending the application of multiple sensors and long-term data acquisition to further validate its effectiveness in the structural health monitoring area. To achieve this, hardware improvements to make it more compact and easy-to-deploy need to be pursued. This enhancement will enable widespread monitoring of port structures, ensuring efficient and scalable data acquisition. Continuous field applications will be conducted to secure stable data acquisition, identify potential improvements, and validate the robustness of the system. Such long-term application will pave the way for a reliable and innovative monitoring system that meets the demands of real-world port environments.

Additionally, in the object detection aspect, exploring state-of-the-art models and leveraging the continuously collected field data will be critical for enhancing model performance, especially under challenging weather conditions. The cloud-based architecture of the system allows for easy integration of these advancements, facilitating ongoing model training and improvements in accuracy. Moreover, development of refining techniques to identify optimal sensor placement position on structures, ensuring that the data collected are both accurate and meaningful for the intended analyses, would be required.

Setting appropriate thresholds for measured data, potentially utilizing finite element analysis (FEA), is another area of focus. This approach can help develop a comprehensive digital twin of port structures, which can significantly enhance predictive maintenance and

structural integrity management. Furthermore, algorithms and deep learning techniques for identifying structural damage based on the acquired data will be developed, with the goal of integrating these tools into the cloud service. This will enable the development of real-time dashboards and automated alerts, providing facility managers with critical insights into the condition of port infrastructure.

Author Contributions: All authors contributed to the main idea of this paper. Conceptualization, J.P. (Jongwoong Park) and J.M.; Software, J.S. and J.P. (Jongwoong Park); Validation, J.S.; Formal analysis, J.W.; Investigation, J.P. (Junyoung Park); Resources, J.M.; Data curation, J.S.; Writing—original draft, J.S.; Writing—review and editing, J.W., J.M., and J.P. (Jongwoong Park); Visualization, J.P. (Junyoung Park); Project administration, J.M. and J.P. (Jongwoong Park); Funding acquisition, J.M. and J.P. (Jongwoong Park). All authors have read and agreed to the published version of the manuscript.

Funding: This research was supported by the Korea Institute of Marine Science & Technology Promotion (grant number 20210659] funded by the Ministry of Oceans and Fisheries, and by the Chung-Ang University Graduate Research Scholarship in 2023. Additional support was provided by the National R&D Project for Smart Construction Technology (RS-2020-KA156007), funded by the Korea Agency for Infrastructure Technology Advancement under the Ministry of Land, Infrastructure, and Transport, and managed by the Korea Expressway Corporation.

Institutional Review Board Statement: Not applicable.

Informed Consent Statement: Not applicable.

Data Availability Statement: Data is contained within the article.

Acknowledgments: Special thanks to Incheon Port Authority (IPA) for their cooperation.

Conflicts of Interest: The authors declare no conflicts of interest.

References

1. Gharehbaghi, V.R.; Noroozinejad Farsangi, E.; Noori, M.; Yang, T.Y.; Li, S.; Nguyen, A.; Málaga-Chuquitaype, C.; Gardoni, P.; Mirjalili, S. A Critical Review on Structural Health Monitoring: Definitions, Methods, and Perspectives. *Arch. Comput. Methods Eng.* **2021**, *29*, 2209–2235. [CrossRef]
2. Roubos, A.A.; Allaix, D.L.; Schweckendiek, T.; Steenbergen, R.D.J.M.; Jonkman, S.N. Time-dependent reliability analysis of service-proven quay walls subject to corrosion-induced degradation. *Reliab. Eng. Syst. Saf.* **2020**, *203*, 107085. [CrossRef]
3. Yang, Y.-C.; Ge, Y.-E. Adaptation strategies for port infrastructure and facilities under climate change at the Kaohsiung port. *Transp. Policy* **2020**, *97*, 232–244. [CrossRef]
4. Choi, J.; Lee, Y.; Kim, T.; Jung, J.; Choi, H.T. Development of a ROV for visual inspection of harbor structures. In Proceedings of the 2017 IEEE Underwater Technology (UT), Busan, Republic of Korea, 21–24 February 2017.
5. Behrje, U.; Isokeit, C.; Meyer, B.; Ehlers, K.; Maehle, E. AUV-based Quay Wall Inspection Using a Scanning Sonar-based Wall Following Algorithm. In Proceedings of the OCEANS 2022, Chennai, India, 21–24 February 2022; pp. 1–9.
6. Hake, F.; Göttert, L.; Neumann, I.; Alkhatib, H. Using Machine-Learning for the Damage Detection of Harbour Structures. *Remote Sens.* **2022**, *14*, 2518. [CrossRef]
7. Korff, M.; Venmans, A.; Stoppelman, P. City Scale InSAR Monitoring of (Buildings Behind) Quay Walls. In Proceedings of the 2021 IEEE International Geoscience and Remote Sensing Symposium IGARSS, Brussels, Belgium, 11–16 July 2021; pp. 1966–1969.
8. Venmans, A.A.M.; op de Kelder, M.; de Jong, J.; Korff, M.; Houtepen, M. Reliability of InSAR satellite monitoring of buildings near inner city quay walls. *Proc. Int. Assoc. Hydrol. Sci.* **2020**, *382*, 195–199. [CrossRef]
9. Hedayati, M.R.; Amidian, A.A.; Amiri, M.H.; Khodadadi, F. Fiber Bragg Grating (FBG) Sensing Network Condition Monitoring of Harbour and Jetty Structures in Iran. *ICSES Trans. Comput. Netw. Commun. (ITCNC)* **2018**, *4*, 11–16.
10. Jo, B.W.; Jo, J.H.; Khan, R.M.A.; Kim, J.H.; Lee, Y.S. Development of a Cloud Computing-Based Pier Type Port Structure Stability Evaluation Platform Using Fiber Bragg Grating Sensors. *Sensors* **2018**, *18*, 1681. [CrossRef] [PubMed]
11. Moerman, W.; Taerwe, L.; De Waele, W.; Degrieck, J.; Himpe, J. Measuring Ground Anchor Forces of a Quay Wall with Bragg Sensors. *J. Struct. Eng.* **2005**, *131*, 322–328. [CrossRef]
12. Zarafshan, A.; Iranmanesh, A.; Ansari, F. Vibration-Based Method and Sensor for Monitoring of Bridge Scour. *J. Bridge Eng.* **2012**, *17*, 829–838. [CrossRef]
13. Dang, V.-H.; Le-Nguyen, K.; Nguyen, T.-T. Semi-supervised vibration-based structural health monitoring via deep graph learning and contrastive learning. *Structures* **2023**, *51*, 158–170. [CrossRef]
14. Xiang, Z.-Q.; Wang, J.-T.; Wang, W.; Pan, J.-W.; Liu, J.-F.; Le, Z.-J.; Cai, X.-Y. Vibration-based health monitoring of the offshore wind turbine tower using machine learning with Bayesian optimisation. *Ocean Eng.* **2024**, *292*, 116513. [CrossRef]

15. Fan, Y.; Zhang, X.; Cheng, E.; Qin, C.; Qin, N.; Wu, J.; Guo, X.; Chen, H.; Guo, T. 1D in-situ convolution system based on vibration signal for real-time structural health monitoring. *Nano Energy* **2024**, *127*, 109694. [CrossRef]
16. Bel-Hadj, Y.; Weil, M.; Weijtjens, W.; Devriendt, C. Experimental validation of automated OMA and mode tracking for structural health monitoring of transmission towers. *Struct. Health Monit.* **2024**. [CrossRef]
17. Kamariotis, A.; Chatzi, E.; Straub, D. Value of information from vibration-based structural health monitoring extracted via Bayesian model updating. *Mech. Syst. Signal Process.* **2022**, *166*, 108465. [CrossRef]
18. Min, J.Y. Smart Maintenance Technology of Port Facilities. *KICTzine* **2022**, *2*, 30–35.
19. Analog Devices. ADXL354 Datasheet and Product Info. Available online: https://www.analog.com/en/products/adxl354.html (accessed on 19 August 2024).
20. Magda, W. Elastic Fender-Dolphin Interaction for Economic Design of Berthing Dolphins. *J. Waterw. Port Coast. Ocean Eng.* **2019**, *145*. [CrossRef]
21. Ren, S.; He, K.; Girshick, R.; Sun, J. Faster R-CNN: Towards Real-Time Object Detection with Region Proposal Networks. *IEEE Trans. Pattern Anal. Mach. Intell.* **2017**, *39*, 1137–1149. [CrossRef] [PubMed]
22. Raspberry Pi Ltd. Raspberry Pi 3 Model B+ Datasheet and Product Info. Available online: https://www.raspberrypi.com/products/raspberry-pi-3-model-b-plus/ (accessed on 19 August 2024).
23. Raspberry Pi Ltd. Raspberry Pi 4 Model B Datasheet and Product Info. Available online: https://www.raspberrypi.com/products/raspberry-pi-4-model-b/specifications/ (accessed on 19 August 2024).
24. Analog Devices. LT3652 Datasheet and Product Info. Available online: https://www.analog.com/en/products/lt3652.html (accessed on 19 August 2024).
25. EPSON. M-A352AD Datasheet and Product Info. Available online: https://global.epson.com/products_and_drivers/sensing_system/acc/a352/ (accessed on 19 August 2024).
26. Liu, C.; Park, J.-W.; Spencer, B.F.; Moon, D.-S.; Fan, J. Sensor fusion for structural tilt estimation using an acceleration-based tilt sensor and a gyroscope. *Smart Mater. Struct.* **2017**, *26*, 105005. [CrossRef]
27. Sensirion. SHT30 Datasheet and Product info. Available online: https://sensirion.com/products/catalog/SHT30-DIS-F (accessed on 19 August 2024).
28. Lightware. LW20 Datasheet and Product info. Available online: https://lightwarelidar.com/shop/lw20-c-100-m/ (accessed on 19 August 2024).
29. PJRC. Teensy 4.0 Datasheet and Product info. Available online: https://www.pjrc.com/store/teensy40.html (accessed on 19 August 2024).
30. m2m2net. LM6 Datasheet and Product info. Available online: https://www.m2mnet.net/products/read.jsp?no=18&code=202103154e420758b7 (accessed on 19 August 2024).
31. He, K.M.; Zhang, X.Y.; Ren, S.Q.; Sun, J. Deep Residual Learning for Image Recognition. In Proceedings of the 2016 IEEE Conference on Computer Vision and Pattern Recognition (CVPR), Las Vegas, NV, USA, 27–30 June 2016; pp. 770–778. [CrossRef]
32. Thorlabs. PRMTZ8/M Datasheet and Product Info. Available online: https://www.thorlabs.com/thorproduct.cfm?partnumber=PRMTZ8/M (accessed on 19 August 2024).

Disclaimer/Publisher's Note: The statements, opinions and data contained in all publications are solely those of the individual author(s) and contributor(s) and not of MDPI and/or the editor(s). MDPI and/or the editor(s) disclaim responsibility for any injury to people or property resulting from any ideas, methods, instructions or products referred to in the content.